SARM1 promotes neuroinflammation and inhibits neural regeneration after spinal cord injury

Huitao Liu
The First Affiliated Hospital of Wenzhou Medical University
Jingjing Zhang
Wenzhou Medical University
Xingxing Xu
Wenzhou Medical University
Danlu Yang
Wenzhou Medical University
Changnan Xie
The First Affiliated Hospital of Wenzhou Medical University
Mengxian Jia
The First Affiliated Hospital of Wenzhou Medical University
Wenbin Zhang
The First Affiliated Hospital of Wenzhou Medical University
Xiya Shen
Wenzhou Medical University
Lingting Jin
Wenzhou Medical University
Sheng Lu
The First Affiliated Hospital of Wenzhou Medical University
Fayi Li
The First Affiliated Hospital of Wenzhou Medical University
Wangfei Wang
The First Affiliated Hospital of Wenzhou Medical University
Xiaomei Bao
Wenzhou Medical University
Sijia Li
Wenzhou Medical University
Minyu Zhu
The First Affiliated Hospital of Wenzhou Medical University
Wei Wang
Wenzhou Medical University
Ying Wang

Zhejiang Provincial People's Hospital of Hangzhou Medical College

Zhihui Huang (hzhzju021@163.com)

The First Affiliated Hospital of Wenzhou Medical University

Honglin Teng

The First Affiliated Hospital of Wenzhou Medical University

Research

Keywords: SARM1, spinal cord injury, neuroinflammation, neural regeneration, axonal degeneration

Posted Date: June 2nd, 2020

DOI: https://doi.org/10.21203/rs.3.rs-32464/v1

Abstract

Background

Axonal degeneration is a common pathological feature in many acute and chronic neurological diseases such as spinal cord injury (SCI). SARM1 (sterile alpha and TIR motif containing 1), the fifth TLR (Toll-like receptor) adaptor, has diverse functions in the immune and nervous systems, and recently has been identified as a key mediator of Wallerian degeneration (WD). However, the detailed functions of SARM1 after SCI still remain unclear.

Methods

Modified Allen's method was used to establish a contusion model of SCI in mice. Furthermore, to address the function of SARM1 after SCI, mice that *SARM1* was conditionally knockout (CKO) in the central nervous system (CNS), namely *SARM1*^{Nestin}-CKO mice, were successfully generated. And to explore the potential of clinical application, FK866, an inhibitor of SARM1, was used to further verify the phenomenon and mechanism.

Results

We found that SARM1 was mainly detected in neurons and was upregulated in neurons at early stage after SCI. And *SARM1*^{Nestin}-CKO mice displayed normal development of the spinal cords and motor function. Interestingly, conditional deletion of *SARM1* in neurons promoted the recovery of behavior performance after SCI. Mechanistically, conditional deletion of *SARM1* in neurons promoted neuronal regeneration at intermediate phase after SCI, and reduced neuroinflammation at SCI early phase, which may through downregulation of NF-κB signaling after SCI. Finally, FK866 reduced neuroinflammation and promoted neuronal regeneration after SCI.

Conclusion

Our results indicate that SARM1-mediated prodegenerative pathway and neuroinflammation promotes the pathological progress of SCI and anti-SARM1 therapeutics are a viable and promising approach for preserving neuronal function after SCI.

Background

Spinal cord injury (SCI) is a severe central nervous system (CNS) damage resulting in a motor and sensory dysfunction, which may cause a permanent paralysis [1]. The therapies of SCI mainly include surgeries, medications and rehabilitation treatments, however, clinical improvements in patients are still

limited and not satisfactory [2]. This is largely due to the unique pathophysiology of SCI with the primary injury followed by a progressive secondary injury [1]. In general, the primary injury is the result of physical forces including compression, shearing, laceration and acute stretch/distraction that induced by the initial traumatic events, and often determines the injury severity of SCI. The primary injury is followed by a cascade of secondary injury events that characterized by multiple injury processes including inflammation, glutamate excitotoxicity, apoptosis and free radical-induced cell death, and serves to expand the zone of injured neural tissue and exacerbates neurological deficits and outcomes [3]. The inflammatory responses including the activation of resident microglia, recruitment of macrophages, neutrophils and lymphocytes from the bloodstream to the injury site, lead to profound neuropathological consequences such as neuronal death as well as axonal degeneration and demyelination, and the formation of glial scars [4]. Although extensive studies have focused on the pathophysiological mechanism of SCI and it has been long recognized that axonal degeneration represents a key pathological feature, the pathogenesis of SCI and the intriguing links between axonal degeneration, neuroinflammation, synaptic growth and cell death after SCI still remain unclear.

A number of studies carried out in animals and human beings suggest that after SCI, the distal stumps of the long injury axons are irreversibly damaged and undergo a degenerative process, which is called Wallerian degeneration (WD), while the proximal stumps retract [5, 6]. WD is a form of programmed self-destruction process that promotes axon breakdown in neurodegenerative diseases and axonal injury [7]. SARM1 is a recently identified key mediator of WD. SARM1 belongs to the TLR adaptor family, and encodes a protein with domains of sterile alpha motif (SAM) and armadillo motif (ARM), thus named SARM and renamed as SARM1 for a Toll/interleukin-1 receptor (TIR) domain is annotated in the C-terminal region [8–10]. The properties and biological functions of SARM1 have been investigated in the immune and nervous systems in the past decades [11–14]. Accumulating studies have shown that SARM1 plays multiple roles in defense of pathogen infection and brain development. On the one hand, human SARM1 negatively regulates MYD88-and TRIF-dependent TLRs signaling in immune responses [15, 16]. On the other hand, SARM1 influence cell death and axonal degeneration, therefore, mediates the neurodegenerative processes of WD [17, 18]. Using *SARM1* knockout mice, it has been demonstrated that loss of SARM1 in neurons prevents cell death under oxygen and glucose deprivation stress [13]. Loss of SARM1 effectively suppresses WD for weeks after axotomy, indicating that SARM1 plays a critical role in WD [14]. In the CNS, lack of SARM1 in mice improves functional outcome and attenuates traumatic axonal injury [19], however, loss of SARM1 does not suppress axonal degeneration in $SOD1^{G93A}$ mouse model of amyotrophic lateral sclerosis (ALS) [20]. Interestingly, recent studies have shown that SARM1 regulates neuronal intrinsic immune response to traumatic axonal injuries in the sciatic nerve injury model [21]. These results suggest that SARM1 plays differential roles under different axonal injury models. However, the exact functions of SARM1 and the underlying mechanisms after SCI still remains poorly understood. Moreover, due to the diverse functions of SARM1, it is necessary to make mice that SARM1 was conditionally knockout (CKO) to address the detailed functions of SARM1 under different pathological conditions.

In the present studies, we examined the roles of SARM1 after SCI. We found that SARM1 was upregulated in neurons of the spinal cords at early stage after SCI, and conditional deletion of *SARM1* in neurons reduced neuroinflammation at SCI early phase through NF-κB signaling, and promoted axonal regeneration at SCI intermediate phase through mitigating demyelination. Moreover, similar results were obtained by FK866 (an inhibitor of SARM1) treatment under SCI, which may help to develop new strategies for the treatment of SCI.

Methods

Animals and mouse breeding

SARM1 ^{Nestin} -CKO conditional knockout mice were generated by crossing the floxed *SARM1* allele (*SARM1*$^{f/f}$) mice with *Nestin-Cre* transgenic mice (003771, from The Jackson Laboratory; donated by Dr Rudiger Klein), which expresses Cre recombinase in neural stem cells under the control of the nestin promoter and conditional knockout genes in neural stem cells and as well as their derivatives including neurons and astrocytes [22]. *SARM1*$^{f/f}$ mice were obtained by crossing between *SARM1*$^{f/w}$ mice, which were generated by Shanghai Biomodel Organism Science & Technology Development Co., Ltd. A targeting vector containing the first two exons of the *SARM1* gene was created by recombineering. Briefly, transformed ES colonies were screened by long-template PCR with the following primer sets: P5F (5'-GGAGTTATAGAGGATCACGAGCCAC – 3') and P5R (5'- GGCCTACCCGCTTCCATTGCTC – 3') to generate a 5.1-kb band for positive clones; P3F (5'- CCGTGCCTTCCTTGACCCTGG – 3') and P3R (5'-AGCCTTTGCCCACTGAGACATC – 3') to generate a 4.7-kb band for positive clones. Successfully targeted ES clones (confirmed by both 5'PCR and 3'PCR) were microinjected into C57BL/6 blastocysts. Germline transmission from generated chimeric offspring was confirmed by long-template PCR. Mice carrying the targeted allele were bred to Flp recombinase transgenic mice to remove the FRT-flanked Neo cassette and to generate the *SARM1* flox mice. Genomic DNAs extracted from tail biopsies were genotyped with a PCR primer set (P1: 5'- AGCAACAAGCACTCTGAATGG – 3', P2: 5'- AGATCACGCCTAGACCGATG – 3') that generated a 466-bp band from the *wild-type* allele, a 500-bp band from the *SARM1* floxed allele. *Flp* was isolated by crossing *SARM1*$^{f/w}$; *Flp* mice with *wild-type* mice. Genomic DNAs extracted from tail biopsies were genotyped with a PCR primer set (PA: 5'- CACTGATATTGTAAGTAGTTTGC – 3', PB: 5'-CTAGTGCGAAGTAGTGATCAGG – 3') that generated no band from the *wild-type* allele, a 715-bp band from the *Flp* allele. Nestin-Cre-tdTomato reporter (*Nestin-Cre*$^{+/-}$; *Ai14*) mice were generated by crossing the floxed tdTomato at Rosa 26 locus allele (*Ai14*) with *Nestin-Cre* transgenic mice. All *wild-type*, *SARM1*$^{f/w}$, *SARM1*$^{f/f}$, *Nestin-Cre*$^{+/-}$; *SARM1*$^{f/w}$, *SARM1*^{Nestin}-CKO and *Nestin-Cre*$^{+/-}$; *Ai14* mice were maintained in C57BL/6 strain background. For all experiments, 8–12 weeks old male mice were used unless specifically stated. All experimental animals were approved by the Laboratory Animals Ethics Committee of Wenzhou Medical University.

SCI surgical procedures

All of the animals (2 M male *wild-type*, *SARM1*$^{f/f}$ and *SARM1*^{Nestin}-CKO mice) underwent general anesthesia (20 ml/kg) by intraperitoneal injection of avertin (2, 2, 2-tribromoethanol, Sigma-Aldrich) in 0.9% saline solution. Surgical procedures were described previously [23, 24]. Briefly, a laminectomy from T8 to T10 of spinal cords was performed on a surgical microscope (Nikon SMZ745) and a mouse spinal cord adapter. Spinal cord was contused in T9 by a weight (10 g) from 5 cm height on a mouse spinal cord impactor (RWD, 68094). After SCI, the bladder was manually evacuated twice daily until the restoration urinating function. In sham group, all animals were subjected to laminectomy alone. All animals were randomly distributed into the following groups and evaluated blind to genotype and experimental condition. Mice were utilized to assess histological, biochemical and behavioral function procedures as described below.

Behavioral analysis

Mice were evaluated using four behavioral experiment assays to assess hindlimb functions as previously described [25].

Open-field locomotor task

The objective of this evaluation was to assess gross voluntary use of the hindlimbs, and did not attempt to define subtle differences in usage that might be correlated with specific neural mechanisms that might underlie dysfunctions. We used a simple six-point scale, as described before [26]. All animals were evaluated in an open field by the same one or two observers blind to the experimental condition and received a score for gross voluntary movement of each hindlimb using an operationally defined six-point scale: (0) no voluntary hindlimb movement, (1) little voluntary hindlimb movement, (3) hindlimb assisted in occasional weight support and plantar placement but not in stepping, (4) hindlimb used for weight support and stepping, but obvious disability, and (5) hindlimb function essentially normal.

Footprint analysis

To assess the athletic ability of forelimbs and hindlimbs, mice were running along a paper-lined runway, as described before [27, 28]. Each forelimb and hindlimb was brushed with black (forelimbs) and red (hindlimbs) nontoxic ink, and qualitative analyzed plantar stepping, stride length and width, and overall stepping ability.

Rotarod performance

To evaluate the function of balance, grip strength and motor coordination, animals were put in a single-lane rotarod (Anhui Zhenghua Biological Instrument Equipment, YLS-10A) for three trials per session, which was set for 3 to 30 rpm over 180 sec, and scored on seconds to fall.

Pole test

To evaluate the ability of balance and coordination, animals were placed on a 50 cm-high pole and the time all four limbs land on were recorded. When the animal paused and could not turn but instead

descended with a lateral body position, the trial was repeated. Each trial was scored individually and averaged for a final score per session.

Western blot

Spinal cords and other nerve tissues were lysed in the lysis buffer: ice-cold RIPA Buffer (P0013B, Beyotime), 100 mM NaF, 100 mM Na_3VO_4, 100 mM PMSF (ST506, Beyotime), and incubated at 4 ℃ for 30 min, and centrifuged at 12, 000 rpm for 30 min, and extracted with 5 · loading buffer (P1040, Solarbio). Finally, the lysates were boiled at 100 ℃ for 10 min. The samples were separated using 8%, 10% or 12% sodium dodecyl sulfate-polyacrylamide gel electrophoresis (SDS-PAGE) and transferred onto nitrocellulose membranes (Life sciences, USA). After blocking in 5% skim milk (232100, BD Bioscience) for 1.5 h, the immunoblots were incubated with different primary antibodies for overnight at 4 ℃. Primary antibodies included rabbit mouse anti-β-actin (A5316, Sigma-Aldrich, 1:10, 000), mouse anti-MBP (ab62631, Abcam, 1:1, 000), rabbit anti-SARM1 (ab226930, Abcam, 1:1, 000), rabbit anti-NF-κB (p65) (ab16502, Abcam, 1:1, 000), rabbit anti-IKB-α (ab32518, Abcam, 1:1, 000), rabbit anti-p-JNK (#4668, Cell Signaling, 1:1, 000), rabbit anti-JNK (bs-2592R, Bioss, 1:1, 000), rabbit anti-c-Jun (bs-0670R, Bioss, 1:1, 000), rabbit anti-NF (ab8135, Abcam, 1:1, 000). Using the secondary antibodies, goat anti-mouse IgG-HRP (31460, Pierce, 1:5, 000) or goat anti-rabbit IgG-HRP (31420, Pierce, 1:5, 000), for 1.5 h. The western blots were detected by the ECL detection kit (Bio-Rad, USA). Subsequently, blots were analyzed using Quantity One software (Bio-Rad, USA).

Nissl staining

Nissl staining was performed as previously described [29]. After mice were perfused with 0.1 mol/L PBS followed by 4% paraformaldehyde (PFA), the spinal cords were immersed in 4% PFA for 24 h and transferred to 30% sucrose solution until they sank. Subsequently, the spinal cords were cut into 20-um-thick transverse and horizontal sections using a freezing microtome (Thermo, USA). After the sections were incubated with 0.1% cresyl violet for 5 min at room temperature, the sections were rinsed in double distilled water followed by 95% ethanol, dehydrated in 100% ethanol and cleared in xylene, and covered by neutral resins. The images were acquired with a microscope (Nikon, Tokyo, Japan) and the ventral horn neurons were counted with ImageJ software (Media Cybernetics, Bethesda, MD, USA). Quantitative analysis of histological staining and fluorescence was used by Image J.

Hematoxylin-Eosin (HE) staining

Briefly, after perfusion with 0.1 M PBS followed by 4% PFA, the spinal cords of mice were immersed in 4% PFA for 24 h and transferred to 30% sucrose solution until they sank. Subsequently, the spinal cords were embedded in OCT (optimal cutting temperature) and were cut into 20 μm-thick transverse sections using a freezing microtome (Thermo, USA). After staining with hematoxylin for 1 min, the sections were washed three times in double distilled water. Then the sections were incubated in the acidic liquid alcohol differentiation for 30 s, staining with eosine for 50 s, followed by 95% ethanol, 100% ethanol, and finally cleared in xylene, and mounted by neutral resins. The images were acquired with a microscope (Nikon, Tokyo, Japan) and quantitative analysis of the images was done by Image J.

Immunostaining

For staining of the spinal cord tissue sections, after fixed 30 min and antigen repaired 30 min at 90℃ by sodium citrate antigen retrieval solution (C1032, Solarbio), the spinal cord tissue sections were processed for immunostaining by 1 h blocking in 5% BSA (4240GR100, Biofroxx) plus 0.3% Triton X-100 (T8200, Solarbio) at room temperature, for overnight incubation with primary antibodies at 4℃, and washed three times in PBS and then were incubated for 1 h at room temperature with appropriate secondary antibodies. Primary antibodies included mouse anti-NeuN (ab177487, Abcam, 1:500), mouse anti-GFAP (MAB360, Millipore, 1:500), goat anti-Iba1 (ab5076, Abcam, 1:500), mouse anti-MBP (ab62631, Abcam, 1:500), rabbit anti-SARM1 (ab226930, Abcam, 1:500), rabbit anti-CD45 (ab10558,Abcam, 1 : 500), rabbit anti-NF (ab8135, Abcam, 1:500). Secondary antibodies included donkey anti-rabbit Alexa Fluor488 (A21206, Invitrogen, 1:1, 000), donkey anti-mouse Alexa Fluor488 (A21202, Invitrogen, 1:1, 000), donkey anti-rabbit Alexa Fluor546 (A10040, Invitrogen, 1:1, 000), donkey anti-mouse Alexa Fluor546 (A10036, Invitrogen, 1:1, 000), donkey anti-goat Alexa Fluor488 (A11055, Invitrogen, 1:1, 000). Images were acquired using confocal microscopes (TCS SP8, Lecia) or microscope (Li2, Nikon) and analyzed with Image J and Photoshop (Adobe).

Quantitative Real-Time PCR (qRT-PCR).

For qRT-PCR, total RNA was extracted from spinal cord of *SARM1*$^{f/f}$ or *SARM1*^{Nestin}-CKO mice at 3 d after SCI using TRIzol™ reagent (#15596026, Ambion) according to the protocol provided by the manufacturer. Then, RNA was reversely transcribed into cDNA with a SuperScript™ One-Step Reverse Transcription Kit (#10928-034, Invitrogen, CA, USA). The expression levels of mRNA were quantified using the iTaq™ Universal SYBR Green Supermix (Bio-Rad, USA) on the Real-Time PCR detection System (Applied Biosystems, USA). Samples were amplified independently at least three times. Relative gene expression was converted using the $2^{-\Delta\Delta Ct}$ method against β-actin. β-actin primer: forward, 5'-GTGACGTTGACATCCGTAAAGA-3' and reverse, 5'- GCCGGACTCATCGTACTCC-3'. NF-κB primer: forward, 5'- AGAGGGGATTTCGATTCCGC – 3' and reverse, 5'- CCTGTGGGTAGGATTTCTTGTTC – 3'. IFN-α primer: forward, 5'- GGATGTGACCTTCCTCAGACTC – 3' and reverse, 5'- ACCTTCTCCTGCGGGAATCCAA – 3'. IFN-β primer: forward, 5'- GCCTTTGCCATCCAAGAGATGC – 3' and reverse, 5'- ACACTGTCTGCTGGTGGAGTTC – 3'. IFN-γ primer: forward, 5'- AGCGGCTGACTGAACTCAGATTGTAG – 3' and reverse, 5'-GTCACAGTTTTCAGCTGTATAGGG – 3'. IL-1β primer: forward, 5'- TGGACCTTCCAGGATGAGGACA – 3' and reverse, 5'- GTTCATCTCGGAGCCTGTAGTG – 3'. MIP-1α primer: forward, 5'-ACTGCCTGCTGCTTCTCCTACA – 3' and reverse, 5'- ATGACACCTGGCTGGGAGCAAA – 3'. TNF-α primer: forward, 5'- GGTGCCTATGTCTCAGCCTCTT – 3' and reverse, 5'- GCCATAGAACTGATGAGAGGGAG – 3'. RANTES primer: forward, 5'- CTCACCATATGGCTCGGACA – 3' and reverse, 5'-ACAAACACGACTGCAAGATTGG – 3'.

Pharmacological interference with the FK866

Sham control and spinal cord injured C57BL/6J mice were treated with FK866 (10 mg/kg i.p., Sigma-Aldrich, catalog #F8557) twice every day until the experiments were terminated [30, 31]. Meanwhile, the control group mice were injected intraperitoneally with the same amount of normal saline.

Statistical analysis

All data presented represent results as mean ± SEM from at least three independent experiments. Statistical analysis was performed using Student's *t*-test or using ANOVA with Bonferroni post-tests. Statistical significance was defined as $P < 0.05$.

Results

SARM1 was upregulated in neurons at early stage after SCI

To investigate the function of SARM1 in spinal cords, we first examined the expression pattern of SARM1 in the spinal cords, and brain regions such as cortex, hippocampus, cerebellum, olfactory bulb and midbrain by Western blot. As shown in Supplementary Fig. S1A, B, we found SARM1 was expressed in the spinal cords, lower than other brain regions. To know the spatial distribution of SARM1 in the spinal cords, double immunostaining of SARM1 and several cell markers including NeuN (a marker of neurons), GFAP (a marker of astrocytes) and Iba1 (a marker of microglia) were performed. We found that SARM1 was mainly detected in $NeuN^+$ neurons, weakly in $GFAP^+$ astrocytes, but not in $Iba1^+$ microglial cells (Supplementary Fig. S1C, D, E). To explore the potential functions of SARM1 after SCI, contusion SCI model was established. As shown in supplementary Fig. S2, the moderate-severe contused injury of spinal cord in T9 was made by a weight (10 g) from 5 cm height that caused a clear injury site and motor impairments. Based on this SCI model, the expression pattern of SARM1 in the spinal cords were detected at different stages after SCI by western blot. We found that the expression of SARM1 protein was significantly upregulated at the 1 d, 3 d at the injury site, and with a peak between 3 d and 7 d after SCI (Fig. 1A, B). To further examine the spatial expression pattern of SARM1 in the spinal cord after SCI, double immunostaining of SARM1 and NeuN were performed. Consistently, SARM1 protein was upregulated and displayed the cytoplasmic location in the $NeuN^+$ neurons at 3 d after SCI and reached the base level at 14 d after SCI (Fig. 1C, D). Taken together, these results indicated that SARM1 was mainly upregulated in neurons at early stages after SCI, which might be involved in the neuronal regeneration.

Normal development of spinal cords in $SARM1^{Nestin}$-CKO mice

To further study the functions of SARM1 in SCI, mice that delete *SARM1* in neurons, $SARM1^{Nestin}$-CKO mice, was generated by crossing floxed *SARM1* allele ($SARM1^{f/f}$) with Nestin-Cre transgenic mice (Supplementary Fig. S3A-C). In order to verify the specific tissue cells of the Nestin-Cre expression, we also generated Nestin-Cre-tdTomato reporter (*Nestin-Cre*$^{+/-}$; *Ai14*) mice. Immunostaining showed that

tdTomato co-stained with NeuN$^+$ neurons and GFAP$^+$ astrocytes in the Nestin-Cre-tdTomato reporter mice (Supplementary Fig. S3D-G), suggesting that *Nestin-Cre* mice were suitable to delete genes in neurons and astrocytes. Indeed, as shown in Supplementary Fig. S3H-I, the expression of SARM1 was dramatically decreased in the spinal cords and other brain regions such as cortex, hippocampus and cerebellum of *SARM1^{Nestin}*-CKO mice, compared with control mice.

We next examined whether the conditional deletion of *SARM1* in neurons affected the spinal cords development and motor functions. As shown in Fig. 2A-F, there was no significant difference in the body weight, neuronal number and neuronal distribution in the spinal cords between *SARM1$^{f/f}$* and *SARM1^{Nestin}*-CKO mice. Moreover, we found that conditional deletion of *SARM1* in neurons did not affect the motor function of mice based on the behavior tests including footprint, rotarod performance and pole test assays (Fig. 2G-J). Taken together, these results indicated that conditional deletion of *SARM1* in neurons did not affect the development of spinal cords and motor functions.

Conditional deletion of SARM1 in neurons promoted the recovery of behavior performance after SCI

The upregulation of SARM1 mainly in neurons led to the speculation for a critical role of SARM1 in neuronal regeneration after SCI. We first examined whether the motor function was affected by *SARM1* deletion in neurons after SCI. As shown in Fig. 3A-C, the footprint behavioral assays showed better performance of *SARM1^{Nestin}*-CKO mice in stride length at 1 d, 3 d, 7d, 14 d, 28 d and stride width at 3 d, 7 d, 14 d, 28 d after SCI. The gross voluntary movement in the open-field locomotor task assays of *SARM1^{Nestin}*-CKO mice was significant longer than *SARM1$^{f/f}$* mice at 3 d, 7 d, 14 d, 28 d, but was not comparable with *SARM1$^{f/f}$* mice at 1 d after SCI (Fig. 3D). However, no significant difference was found in the rotarod performance assays between *SARM1$^{f/f}$* and *SARM1^{Nestin}*-CKO mice (Fig. 3E). Taken together, these results suggested that conditional deletion of *SARM1* in neurons promoted the recovery of motor functions in some behavior tests after SCI.

Conditional deletion of SARM1 in neurons inhibited the loss of neurons and the neuronal degeneration at intermediate phase after SCI

Since SARM1 promotes the Wallerian Degeneration after injury as described previously [32–34], we next examined whether the deletion of *SARM1* in neurons promoted the recovery of motor functions due to the delay in neuronal degeneration after SCI. As expected, NeuN staining showed that the area of injury site and loss of neurons after SCI was significantly decreased in *SARM1^{Nestin}*-CKO mice at 14 d after SCI, compared with *SARM1$^{f/f}$* mice (Fig. 4A). These results suggested that *SARM1* deletion in neurons alleviated the damage of neurons after SCI. Furthermore, we performed the immunostaining of neurofilament (NF) (an axonal regeneration marker) to assess the neural regeneration in *SARM1$^{f/f}$* and *SARM1^{Nestin}*-CKO mice after SCI. As shown in Fig. 4B, C, E, we found the intensity of NF were significantly higher in *SARM1^{Nestin}*-CKO mice at 14 d and 28 d after SCI, compared with the *SARM1$^{f/f}$* mice. The

intensity of myelin basic protein (MBP) (a mature myelin marker) was also significantly higher at 28 d after SCI in *SARM1*^{Nestin}-CKO mice than *SARM1*$^{f/f}$ mice (Fig. 4C, D). Taken together, these results suggested that conditional deletion of *SARM1* in neurons inhibited the loss of neurons and axon degeneration at intermediate (2 w-6 M after SCI) phase after SCI.

Conditional deletion of SARM1 in neurons reduced neuroinflammation at SCI early phase

How does *SARM1* deletion in neurons inhibit the neural degeneration after SCI? Since previous studies have shown that SARM1 regulates neuronal intrinsic immune response to axonal injury [21], thus we next examined whether SARM1 was involved in neuroinflammation after SCI. The spinal cords of *SARM1*$^{f/f}$ and *SARM1*^{Nestin}-CKO mice at 3 d after SCI were collected, because 3 d after SCI was at the early phase and SARM1 has the highest expression as shown above. As shown in Fig. 5A-B, area of hematoma was significantly decreased in *SARM1*^{Nestin}-CKO mice at 3 d after SCI. Again, Nissl staining and HE staining showed that the area of injury site after SCI was significantly decreased, and infiltration of inflammatory cells was also reduced in *SARM1*^{Nestin}-CKO mice at 3 d after SCI (Fig. 5C-G). Finally, we performed the immunostaining of inflammatory cells by several cell markers. Interestingly, we found that the number of inflammatory cells, such as Iba1^{+} microglia, CD45^{+} immune cells and GFAP^{+} astrocytes were significantly decreased in *SARM1*^{Nestin}-CKO mice at 3 d after SCI (Fig. 5H-J, Supplementary Fig. S4). Taken together, these results suggested that conditional deletion of *SARM1* reduced neuroinflammation at SCI early phase, which might promote neural regeneration.

Conditional deletion of SARM1 in neurons reduced the neuroinflammation through downregulation of NF-κB signaling after SCI

How did *SARM1* deletion reduce the inflammation after SCI? Since NF-κB signaling is a main downstream pathway of SARM1, we next detected the expression of probably related proteins as previously described, such as NF-κB, IKB-α, JNK, p-JNK and c-Jun (Fig. 6A). Interestingly, in the spinal cords of *SARM1*$^{f/f}$ mice, NF-κB was significantly increased at all phases after SCI, and IKB-α was significantly increased at 3 d, 7 d, 14 d and 28 d after SCI, however, *SARM1*^{Nestin}-CKO mice failed to increase the level of these proteins (Fig. 6B, C). Meanwhile, MBP protein was significantly higher in *SARM1*^{Nestin}-CKO mice at all phases after SCI, compared with *SARM1*$^{f/f}$ mice (Fig. 6D), which was consistent with the results of *SARM1* deletion in neurons inhibited the axon degeneration. These results suggested that *SARM1* knockout impaired the NF-κB signaling pathway in the spinal cords after SCI. To further support this notion, we next performed the qRT-PCR to examine the transcription level expression of the inflammatory factors. And the mRNA expression levels of NF-κB and IFN-α, IFN-β, IFN-γ, IL-1β, MIP-1α, TNF-α, RANTES were significantly decreased in *SARM1*^{Nestin}-CKO mice at 3 d after SCI, compared with *SARM1*$^{f/f}$ mice (Supplementary Fig. S5). Taken together, *SARM1* deletion in neurons reduced the neuroinflammation after SCI through NF-κB signaling, which may alleviate the neuronal degeneration.

Inhibition of SARM1 by FK866 promoted the neuronal regeneration after SCI

We next examined whether inhibition of SARM1 pathway promoted the neuronal regeneration after SCI. FK866, a feedback inhibitor of SARM1 that raise the levels of nicotinamide (Nam) (an intermediate of energy metabolism) in the axonal compartment [18], was applied in mice after SCI. As expected, as shown in Fig. 7A, B, the footprint and open field assays found that the behavioral recovery was significantly increased in FK866-treated mice, compared with control mice. Furthermore, we found that the number of $Iba1^+$ and $CD45^+$ inflammatory cells was significantly decreased in FK866-treated mice at 3 d after SCI, compared with control mice (Fig. 7C-E), and the intensity of MBP and NF was significantly increased in FK866-treated mice at 28 d after SCI (Fig. 7F-H). Taken together, these results suggested that inhibition of SARM1 by FK866 reduced neuroinflammation and promoted neural regeneration after SCI.

Discussion

In this study, we provide evidence for SARM1's functions after SCI and propose a working model depicted in Fig. 8. In this model, conditional deletion of *SARM1* in neurons or FK866 treatment inhibited the generation of neuroinflammation cells, promoted axonal regeneration and improved the behavioral recovery of motor function after SCI. Mechanistically, *SARM1* knockout delayed the degeneration of neurons and impaired the activation of NF-κB signal pathway to inhibit inflammation after SCI. Collectively, our data demonstrate that SARM1 promotes neuroinflammation and inhibits neural regeneration after SCI.

Previous studies have shown that SARM1 mRNA is highly expressed in the brain, lowly expressed in other tissues such as in spleen and lymph node [35]. In the CNS, SARM1 mRNA is expressed in primary cultured neurons, astrocytes and microglia [35], and SARM1 protein is mainly expressed in neurons in most brain regions such as cortex, hippocampus and cerebellum [36]. Consistent with these previous studies, we also found that SARM1 was highly expressed in neurons, weakly in astrocytes, but not in microglia of the spinal cords and upregulated in neurons after SCI. Since SARM1 has diverse functions and is expressed in several tissues [35–37], to better understand its role in neurons after SCI, conditional deletion of *SARM1* mice in neurons, $SARM1^{Nestin}$-CKO mice, were successfully generated in our study (Supplementary Fig. 3). In these mice, *SARM1* was conditionally knockout in the spinal cords and cortex, hippocampus and cerebellum. Previous studies have shown that *SARM1* knockout mice display defects in neuronal morphogenesis [38] and exhibit abnormal social and cognitive behaviors, but have normal locomotor activity and anxiety behaviors [39]. Consistently, in our study, $SARM1^{Nestin}$-CKO mice displayed normal development of the spinal cords and showed normal locomotor activity (Fig. 2).

Previous studies have demonstrated that axon destruction appears in WD after SCI [40, 41]. Several studies in related fields clearly demonstrated that SARM1 plays an important role in axon degeneration and in traumatic axonal injury. The severed axons from *SARM1* knockout mice exhibited remarkable

longer-term survival both in *vivo* and in *vitro* than *wild-type* mice [14]. SARM1 activation triggers axon degeneration locally via NAD^+ deprivation, and a significant reduction in the number of axonal lesions early after injury was found by genetically ablating *SARM1* or by FK866 treatment [17]. Genetic or pharmacological interference with SARM1 signaling ameliorates early axonal pathology [42]. Consistent with these previous studies, in the present study, we also found that conditional deletion of *SARM1* in neurons reduced the area of injury site and loss of neurons after SCI, and promoted the recovery of motor functions, indicating that loss of SARM1 in neurons promoted the survival of neurons and delayed neuronal degeneration of the spinal cords after SCI (Fig. 4). We also noted that one previous study has shown that loss of SARM1 does not suppress the degeneration of motor neurons in the $SOD1^{G93A}$ mouse model of ALS [20]. The discrepant results may be due to different animal models (ALS vs SCI). It is interesting to test how *SARM1* knockout suppresses the degeneration of motor neurons in future.

Increasing studies have indicated that SARM1 regulates neuronal intrinsic immune response, white matter neuroinflammation, and prion-induced neuroinflammation [21, 43, 44]. Consistent with these studies, in our study, conditional deletion of *SARM1* in neurons reduced inflammatory infiltration and activation of microglia and astrocytes after SCI (Fig. 5 and Supplementary Fig. 4). However, several studies have indicated that neuroinflammation is associated with WD. After CNS injury, WD are inadequate for removing inhibitory myelin debris, and most macrophages show a neurotoxic phenotype and prevent effective growth of long-distance axons [45]. WD was one type of neuroimmune responses, which may support tissue repair [46]. Our findings demonstrated that deletion of *SARM1* in neurons contributed at least in part to the anti-neuroinflammation effect on SCI at early phase, which may promote neural regeneration at intermediate phase after SCI.

FK866, a feedback inhibitor of SARM1, which has been widely used in blocking Nam consumption by inhibiting nicotinamide phosporibosyltransferase (NAMPT) [18, 42]. Previous studies have found that FK866 exerts multiple beneficial effects, including treat cancer, inflammatory diseases and neutrophil-mediated injuries [30, 47–49]. Indeed, FK866 is capable of reducing the secondary inflammatory injury, and partially relieves permanent damage of SCI [50]. Consistently, in our study, inhibition of SARM1 by FK866 inhibited neuroinflammation, promoted neural regeneration and promoted the recovery of behavior performance after SCI (Fig. 7). Therefore, FK866 or its analogue may be effective drug to cure SCI.

In summary, our study identifies SARM1's function in SCI, SARM1 promotes neuroinflammation and inhibits neural regeneration after SCI. Therefore, discovery of inhibitors of SARM1 signaling pathway such as FK866 may be a useful drug target to treat SCI in future.

Conclusions

In conclusion, our results indicate that SARM1-mediated prodegenerative pathway and neuroinflammation promotes the pathological progress of SCI and anti-SARM1 therapeutics are a viable and promising approach for preserving neuronal function after SCI.

Abbreviations

ALS: amyotrophic lateral sclerosis; CKO: conditional knockout; SARM1: sterile alpha and TIR motif containing 1; SCI: spinal cord injury; TLR: Toll-like receptor; WD: Wallerian degeneration.

Declarations

Availability of data and materials

Most of the datasets supporting the conclusions of this article are included within this article and the additional files. The datasets used or analyzed during the current study are available on reasonable request.

Ethics approval and consent to participate

All animal procedures were performed under the guidelines of the institutional review board and the ethics committee of Wenzhou Medical University.

Consent for publication

Not applicable.

Competing interests

The authors declare that they have no competing interests.

Funding

This work was supported by the Natural Science Foundation of Zhejiang Province (LR18C090001, LY18C090004), National Natural Science Foundation (31671071, 81771348, 81971172), Shenzhen-Hong Kong Institute of Brain Science-Shenzhen Fundamental Research Institutions (NYKFKT2019008), the Research Start-up Project by Wenzhou Medical University (grant number 89217022) and the Research Start-up Project by Hangzhou Normal University (4125C5021920453).

Authors' contributions:

Honglin Teng, Zhihui Huang, Xingxing Xu and Ying Wang contributed to the conception and design of the study. Huitao Liu generated the conditional knockout mice, and did most of western blot and immunofluorescent staining experiments. Jingjing Zhang and Xingxing Xu helped to breed mice, and they both contributed to the acquisition and interpretation of the data. Danlu Yang, Changnan Xie, Mengxian Jia, Wenbin Zhang, Xiya Shen, Lingting Jin, Sheng Lu, Fayi Li, Wangfei Wang, Sijia Li, Xiaomei Bao,

Minyu Zhu and Wei Wang contributed to behavioral experiment assays, genotyping and data analysis. Huitao Liu wrote the manuscript. Honglin Teng, Zhihui Huang, Xingxing Xu and Ying Wang contributed to revising the original text.

Acknowledgments

We thank members of the Zhihui Huang laboratory for helpful discussions and suggestions.

References

1. Ahuja CS, Nori S, Tetreault L, Wilson J, Kwon B, Harrop J, et al. Traumatic Spinal Cord Injury-Repair and Regeneration. Neurosurgery. 2017;80:9–22.
2. Silva NA, Sousa N, Reis RL, Salgado AJ. From basics to clinical: a comprehensive review on spinal cord injury. Prog Neurobiol. 2014;114:25–57.
3. Wang JL, Luo X, Liu L. Targeting CARD6 attenuates spinal cord injury (SCI) in mice through inhibiting apoptosis, inflammation and oxidative stress associated ROS production. Aging-Us. 2019;11:12213–35.
4. Mietto BS, Mostacada K, Martinez AM. Neurotrauma and inflammation: CNS and PNS responses. Mediators Inflamm. 2015;2015:1–14.
5. Conforti L, Gilley J, Coleman MP. Wallerian degeneration: an emerging axon death pathway linking injury and disease. Nat Rev Neurosci. 2014;15:394–409.
6. Chen YJ, Nabavizadeh SA, Vossough A, Kumar S, Loevner LA, Mohan S. Wallerian Degeneration Beyond the Corticospinal Tracts: Conventional and Advanced MRI Findings. J Neuroimaging. 2017;27:272–80.
7. Coleman MP, Freeman MR. Wallerian Degeneration, WldS, and Nmnat. Annu Rev Neurosci. 2010;33:245–67.
8. Mink M, Fogelgren B, Olszewski K, Maroy P, Csiszar K. A novel human gene (SARM) at chromosome 17q11 encodes a protein with a SAM motif and structural similarity to Armadillo/beta-catenin that is conserved in mouse, Drosophila, and Caenorhabditis elegans. Genomics. 2001;74:234–44.
9. O'Neill LAJ, Fitzgerald KA, Bowie AG. The Toll-IL-1 receptor adaptor family grows to five members. Trends Immunol. 2003;24:287–90.
10. Mink M, Csiszar K. SARM1: A candidate gene in the onset of hereditary infectious/inflammatory diseases. Clin Immunol. 2005;115:333–4.
11. Liberati NT, Fitzgerald KA, Kim DH, Feinbaum R, Golenbock DT, Ausubel FM. Requirement for a conserved Toll/interleukin-1 resistance domain protein in the Caenorhabditis elegans immune response. Proc Natl Acad Sci U S A. 2004;101:6593–8.
12. Hao Y, Waller TJ, Nye DM, Li J, Zhang Y, Hume RI, et al. Degeneration of Injured Axons and Dendrites Requires Restraint of a Protective JNK Signaling Pathway by the Transmembrane Protein Raw. J

Neurosci. 2019;39:8457–70.

13. Kim Y, Zhou P, Qian L, Chuang JZ, Lee J, Li C, et al. MyD88-5 links mitochondria, microtubules, and JNK3 in neurons and regulates neuronal survival. J Exp Med. 2007;204:2063–74.
14. Osterloh JM, Yang J, Rooney TM, Fox AN, Adalbert R, Powell EH, et al. dSarm/Sarm1 Is Required for Activation of an Injury-Induced Axon Death Pathway. Science. 2012;337:481–4.
15. Carty M, Goodbody R, Schroder M, Stack J, Moynagh PN, Bowie AG. The human adaptor SARM negatively regulates adaptor protein TRIF-dependent Toll-like receptor signaling. Nat Immunol. 2006;7:1074–81.
16. Peng J, Yuan Q, Lin B, Panneerselvam P, Wang X, Luan XL, et al. SARM inhibits both TRIF- and MyD88-mediated AP-1 activation. Eur J Immunol. 2010;40:1738–47.
17. Gerdts J, Brace EJ, Sasaki Y, DiAntonio A, Milbrandt J. SARM1 activation triggers axon degeneration locally via NAD(+) destruction. Science. 2015;348:453–7.
18. Essuman K, Summers DW, Sasaki Y, Mao X, DiAntonio A, Milbrandt J. The SARM1 Toll/Interleukin-1 Receptor Domain Possesses Intrinsic NAD(+) Cleavage Activity that Promotes Pathological Axonal Degeneration. Neuron. 2017;93:1334–43.
19. Henninger N, Bouley J, Sikoglu EM, An J, Moore CM, King JA, et al. Attenuated traumatic axonal injury and improved functional outcome after traumatic brain injury in mice lacking Sarm1. Brain. 2016;139:1094–105.
20. Peters OM, Lewis EA, Osterloh JM, Weiss A, Salameh JS, Metterville J, et al. Loss of Sarm1 does not suppress motor neuron degeneration in the SOD1 (G93A) mouse model of amyotrophic lateral sclerosis. Hum Mol Genet. 2018;27:3761–71.
21. Wang Q, Zhang S, Liu T, Wang H, Liu K, Wang Q, et al. Sarm1/Myd88-5 Regulates Neuronal Intrinsic Immune Response to Traumatic Axonal Injuries. Cell Rep. 2018;23:716–24.
22. Tronche F, Kellendonk C, Kretz O, Gass P, Anlag K, Orban PC, et al. Disruption of the glucocorticoid receptor gene in the nervous system results in reduced anxiety. Nat Genet. 1999;23:99–103.
23. Bellver-Landete V, Bretheau F, Mailhot B, Vallieres N, Lessard M, Janelle ME, et al. Microglia are an essential component of the neuroprotective scar that forms after spinal cord injury. Nat Commun. 2019;10:1–18.
24. Matyas JJ, O'Driscoll CM, Yu L, Coll-Miro M, Daugherty S, Renn CL, et al. Truncated TrkB.T1-Mediated Astrocyte Dysfunction Contributes to Impaired Motor Function and Neuropathic Pain after Spinal Cord Injury. J Neurosci. 2017;37:3956–71.
25. Xie CN, Shen XY, Xu XX, Liu HT, Li FY, Lu S, et al. Astrocytic YAP Promotes the Formation of Glia Scars and Neural Regeneration after Spinal Cord Injury. J Neurosci. 2020;40:2644–62.
26. Fehlings MG, Tator CH. The relationships among the severity of spinal cord injury, residual neurological function, axon counts, and counts of retrogradely labeled neurons after experimental spinal cord injury. Exp Neurol. 1995;132:220–8.

27. Ma M, Basso DM, Walters P, Stokes BT, Jakeman LB. Behavioral and histological outcomes following graded spinal cord contusion injury in the C57Bl/6 mouse. Exp Neurol. 2001;169:239–54.
28. Faulkner JR, Herrmann JE, Woo MJ, Tansey KE, Doan NB, Sofroniew MV. Reactive astrocytes protect tissue and preserve function after spinal cord injury. J Neurosci. 2004;24:2143–55.
29. Wang P, Xie ZD, Xie CN, Lin CW, Wang JL, Xuan LN, et al. AMP-activated protein kinase-dependent induction of autophagy by erythropoietin protects against spinal cord injury in rats. CNS Neurosci Ther. 2018;24:1185–95.
30. Bruzzone S, Fruscione F, Morando S, Ferrando T, Poggi A, Garuti A, et al. Catastrophic NAD + depletion in activated T lymphocytes through Nampt inhibition reduces demyelination and disability in EAE. PLoS One. 2009;4:e7897.
31. Van Gool F, Galli M, Gueydan C, Kruys V, Prevot PP, Bedalov A, et al. Intracellular NAD levels regulate tumor necrosis factor protein synthesis in a sirtuin-dependent manner. Nat Med. 2009;15:206–10.
32. Ahuja CS, Wilson JR, Nori S, Kotter MRN, Druschel C, Curt A, et al. Traumatic spinal cord injury. Nat Rev Dis Primers. 2017;3:17018.
33. Loreto A, Di Stefano M, Gering M, Conforti L. Wallerian Degeneration Is Executed by an NMN-SARM1-Dependent Late Ca(2+) Influx but Only Modestly Influenced by Mitochondria. Cell Rep. 2015;13:2539–52.
34. Loreto A, Hill CS, Hewitt VL, Orsomando G, Angeletti C, Gilley J, et al. Mitochondrial impairment activates the Wallerian pathway through depletion of NMNAT2 leading to SARM1-dependent axon degeneration. Neurobiol Dis. 2020;134:104678.
35. Szretter KJ, Samuel MA, Gilfillan S, Fuchs A, Colonna M, Diamond MS. The immune adaptor molecule SARM modulates tumor necrosis factor alpha production and microglia activation in the brainstem and restricts West Nile Virus pathogenesis. J Virol. 2009;83:9329–38.
36. Lin CW, Liu HY, Chen CY, Hsueh YP. Neuronally-expressed Sarm1 regulates expression of inflammatory and antiviral cytokines in brains. Innate Immun. 2014;20:161–72.
37. Loring HS, Thompson PR. Emergence of SARM1 as a Potential Therapeutic Target for Wallerian-type Diseases. Cell Chemical Biology. 2020;27:1–13.
38. Chen CY, Lin CW, Chang CY, Jiang ST, Hsueh YP. Sarm1, a negative regulator of innate immunity, interacts with syndecan-2 and regulates neuronal morphology. J Cell Biol. 2011;193:769–84.
39. Lin CW, Hsueh YP. Sarm1, a neuronal inflammatory regulator, controls social interaction, associative memory and cognitive flexibility in mice. Brain Behav Immun. 2014;37:142–51.
40. Mittal P, Gupta R, Mittal A, Mittal K. MRI findings in a case of spinal cord Wallerian degeneration following trauma. Neurosciences (Riyadh). 2016;21:372–3.
41. Valencia MP, Castillo M. MRI findings in posttraumatic spinal cord Wallerian degeneration. Clin Imaging. 2006;30:431–3.
42. Ziogas NK, Koliatsos VE. Primary Traumatic Axonopathy in Mice Subjected to Impact Acceleration: A Reappraisal of Pathology and Mechanisms with High-Resolution Anatomical Methods. J Neurosci.

2018;38:4031–47.
43. Zhu C, Li B, Frontzek K, Liu Y, Aguzzi A. SARM1 deficiency up-regulates XAF1, promotes neuronal apoptosis, and accelerates prion disease. J Exp Med. 2019;216:743–56.
44. Marion CM, McDaniel DP, Armstrong RC. Sarm1 deletion reduces axon damage, demyelination, and white matter atrophy after experimental traumatic brain injury. Exp Neurol. 2019;321:113040.
45. Gaudet AD, Popovich PG, Ramer MS. Wallerian degeneration: gaining perspective on inflammatory events after peripheral nerve injury. J Neuroinflammation. 2011;8:110.
46. Chen Q, Shine HD. Neuroimmune processes associated with Wallerian degeneration support neurotrophin-3-induced axonal sprouting in the injured spinal cord. J Neurosci Res. 2013;91:1280–91.
47. Yang S, Ryu JH, Oh H, Jeon J, Kwak JS, Kim JH, et al. NAMPT (visfatin), a direct target of hypoxia-inducible factor-2alpha, is an essential catabolic regulator of osteoarthritis. Ann Rheum Dis. 2015;74:595–602.
48. Busso N, Karababa M, Nobile M, Rolaz A, Van Gool F, Galli M, et al. Pharmacological inhibition of nicotinamide phosphoribosyltransferase/visfatin enzymatic activity identifies a new inflammatory pathway linked to NAD. PLoS One. 2008;3:e2267.
49. Montecucco F, Bauer I, Braunersreuther V, Bruzzone S, Akhmedov A, Luscher TF, et al. Inhibition of nicotinamide phosphoribosyltransferase reduces neutrophil-mediated injury in myocardial infarction. Antioxid Redox Signal. 2013;18:630–41.
50. Esposito E, Impellizzeri D, Mazzon E, Fakhfouri G, Rahimian R, Travelli C, et al. The NAMPT inhibitor FK866 reverts the damage in spinal cord injury. J Neuroinflammation. 2012;9:66.

Supplementary Figure Legends

Supplementary Fig. 1. High expression of SARM1 in neurons of the spinal cords.

(A) Western blot analysis of SARM1 expression in spinal cords and other brain regions of the CNS. **(B)** Quantitative analysis of the relative SARM1 levels (normalized to the spinal cord group) as shown in (A) (n = 5 per group). **(C-E)** Double immunostaining of SARM1 (green), NeuN (red) (C) or GFAP (red) (D) or Iba1(red) (E), and DAPI (blue) in the spinal cords. Images of selected regions (rectangles) in (C-E) were shown at higher magnification. Scale bars, 20 μm. Data were mean ± SEM.

Supplementary Fig. 2. Establishment of the contusion SCI mouse model.

(A) The modified Allen's contusion impactor of SCI in mice. **(B)** The impact-induced contusion (arrow) on the dorsal surface of the spinal cord. **(C)** Gross morphology of 2 M male *wild-type* mice at 1 d after SCI. **(D)** Representative images of the spinal cords with hematoma of *wild-type* mice at different stages after SCI. **(E)** Quantitative analysis of gross voluntary movement in open-field walking assays of *wild-type* mice over a 28-d period after SCI (two-way ANOVA with Bonferroni's post-tests, n = 10 per group). Scale bars, 2 cm (A), 1 mm (B), 1 cm (C). Data were mean ± SEM. $^{***}P < 0.001$.

Supplementary Fig. 3. Identification SARM1^{Nestin}**-CKO mice.**

(A-B) Diagrams showing the strategy used to generate *SARM1^{Nestin}*-CKO mice. **(C)** Genotyping of *SARM1^{Nestin}*-CKO mice. **(D)** A diagram showing the strategy used to generate *Nestin-Cre$^{+/-}$*; *Ai14* mice. **(E)** Images of the whole spinal cords of control (*wild-type*) and *Nestin-cre*; *Ai14* mice. **(F-G)** Immunostaining of NeuN (green) (F) or GFAP (green) (G) in uninjured spinal cords of *Nestin-Cre$^{+/-}$*; *Ai14* mice. **(H)** Western blot analysis of SARM1 expression in the spinal cords and various brain regions of 2M male *SARM1$^{f/f}$* and *SARM1^{Nestin}*-CKO mice. **(I)** Quantitative analysis of the relative SARM1 levels as shown in (H) (two-tailed paired Student's *t*-test, $n = 4$ per group, normalized to *SARM1$^{f/f}$* group). Images of selected regions (rectangles) in (F) and (G) were shown at higher magnification. Scale bars, 3 mm (E), 20 μm (F, G). Data were mean ± SEM. $^{***}P < 0.001$.

Supplementary Fig. 4. GFAP$^+$ astrocytes were significantly decreased in SARM1^{Nestin}**-CKO mice at 3 d after SCI.**

(A) Double immunostaining of GFAP (red) and DAPI (blue) in injured spinal cords of *SARM1$^{f/f}$* and *SARM1^{Nestin}*-CKO mice at 3 d after SCI. **(B)** Quantitative analysis of the intensity of GFAP$^+$ cells as shown in (A) (two-tailed unpaired Student's *t*-test, $n = 3$ per group, normalized to *SARM1$^{f/f}$* group). Dashed lines indicated the outline of the injury sites. Images of selected regions (rectangles) in (A) were shown at higher magnification. Scale bars, 20 μm. Data were mean ± SEM. $^{*}P < 0.05$.

Supplementary Fig. 5. Transcription level expression of inflammatory factors in injured spinal cord of SARM1$^{f/f}$ **and** SARM1^{Nestin}**-CKO mice at 3 d after SCI.**

(A-H) Real time PCR analysis showed the relative NF-κB (A), IFN-α (B), IFN-β (C), IFN-γ (D), IL-1β (E), MIP-1α (F), TNF-α (G) and RANTES (H) mRNA level of injured spinal cords of *SARM1$^{f/f}$* and *SARM1^{Nestin}*-CKO mice at 3 d after SCI (two-tailed unpaired Student's *t*-test, $n = 4$ per group, normalized to *SARM1$^{f/f}$* group). Data were mean ± SEM. $^{*}P < 0.05$, $^{**}P < 0.01$, $^{***}P < 0.001$.

Figures

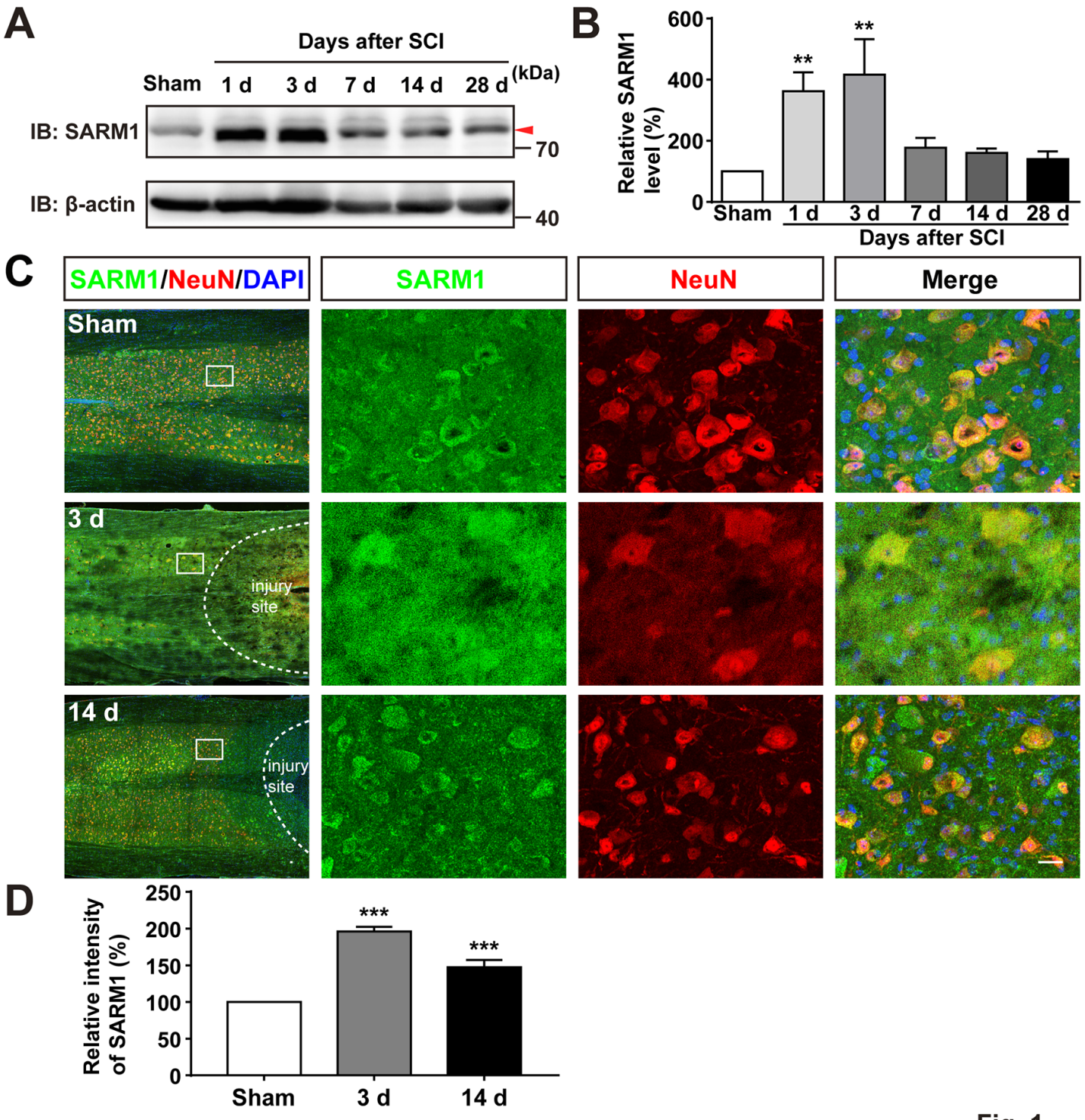

Fig. 1

Figure 1

Fig. 1. SARM1 was upregulated in neurons at early stage after SCI. (A) Western blot analysis of SARM1 expression in the spinal cords at different stages after SCI. (B) Quantitative analysis of the relative SARM1 level (normalized to sham group) as shown in (A) (one-way ANOVA with Bonferroni's post-tests, n = 5 per group). (C) Double immunostaining of SARM1 (green) and NeuN (red) in coronal sections of uninjured spinal cords and injured spinal cords at 3 d, 14 d after SCI. (D) Quantitative analysis of the relative fluorescent intensity of SARM1 level (normalized to sham group) at different stages after SCI as

shown in (C) (one-way ANOVA with Bonferroni's post-tests, n = 5 coronal sections per group). Dashed lines indicated the outline of the injury sites. Images of selected regions (rectangles) in (C) were shown at higher magnification. Scale bars, 20 μm. Data were mean ± SEM. **P < 0.01, ***P < 0.001.

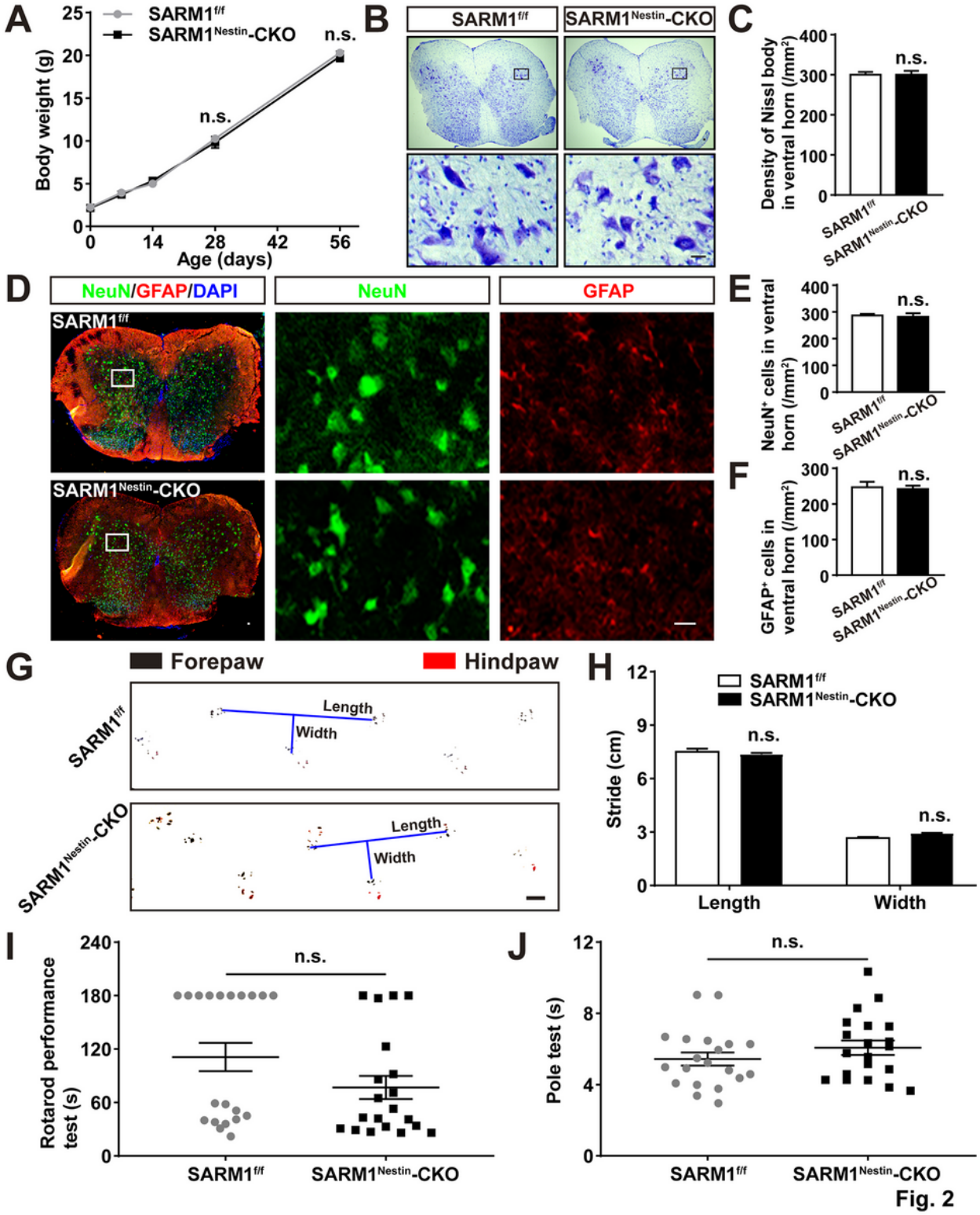

Figure 2

Normal development of spinal cords of SARM1Nestin-CKO mice. (A) Quantitative analysis of the body weight of SARM1f/f and SARM1Nestin-CKO mice at dif-ferent developmental stages (two-way ANOVA

with Bonferroni's post-tests, n = 3 per group). (B) Nissl staining images showing the nissl bodies in the ventral horn of the spinal cords of 2 M male SARM1f/f and SARM1Nestin-CKO mice. (C) Quantitative analysis of the number of neurons as shown in (B) (two-tailed unpaired Student's t-test, n = 6 per group). (D) Double immunostaining analysis of NeuN (green) and GFAP (red) in the ventral horn of the spinal cords of 2 M male SARM1f/f and SARM1Nestin-CKO mice. (E-F) Quantitative analysis of the number of NeuN+ or GFAP+ cells as shown in (D) (two-tailed unpaired Student's t-test, n = 6 per group). (G) Representative footprint images of 2 M male SARM1f/f and SARM1Nestin-CKO mice. (H) Quantitative analysis of stride length and stride width in footprint assays of 2 M male SARM1f/f and SARM1Nestin-CKO mice as shown in (G) (two-tailed unpaired Student's t-test, n = 6 per group). (I) Quantitative analysis of the time taken to fall in rotarod perfor-mance test of 2 M male SARM1f/f and SARM1Nestin-CKO mice (two-tailed unpaired Student's t-test, n = 20 per group). (J) Quantitative analysis of the time all the four limbs took to land on in the pole test of 2 M male SARM1f/f and SARM1Nestin-CKO mice (two-tailed unpaired Student's t-test, n = 20 per group). Images of selected regions (rectangles) in (B) and (D) were shown at higher magnification. Scale bars, 20 μm (B, D), 1cm (G). Data were mean ± SEM. n.s., not significant ($P > 0.05$).

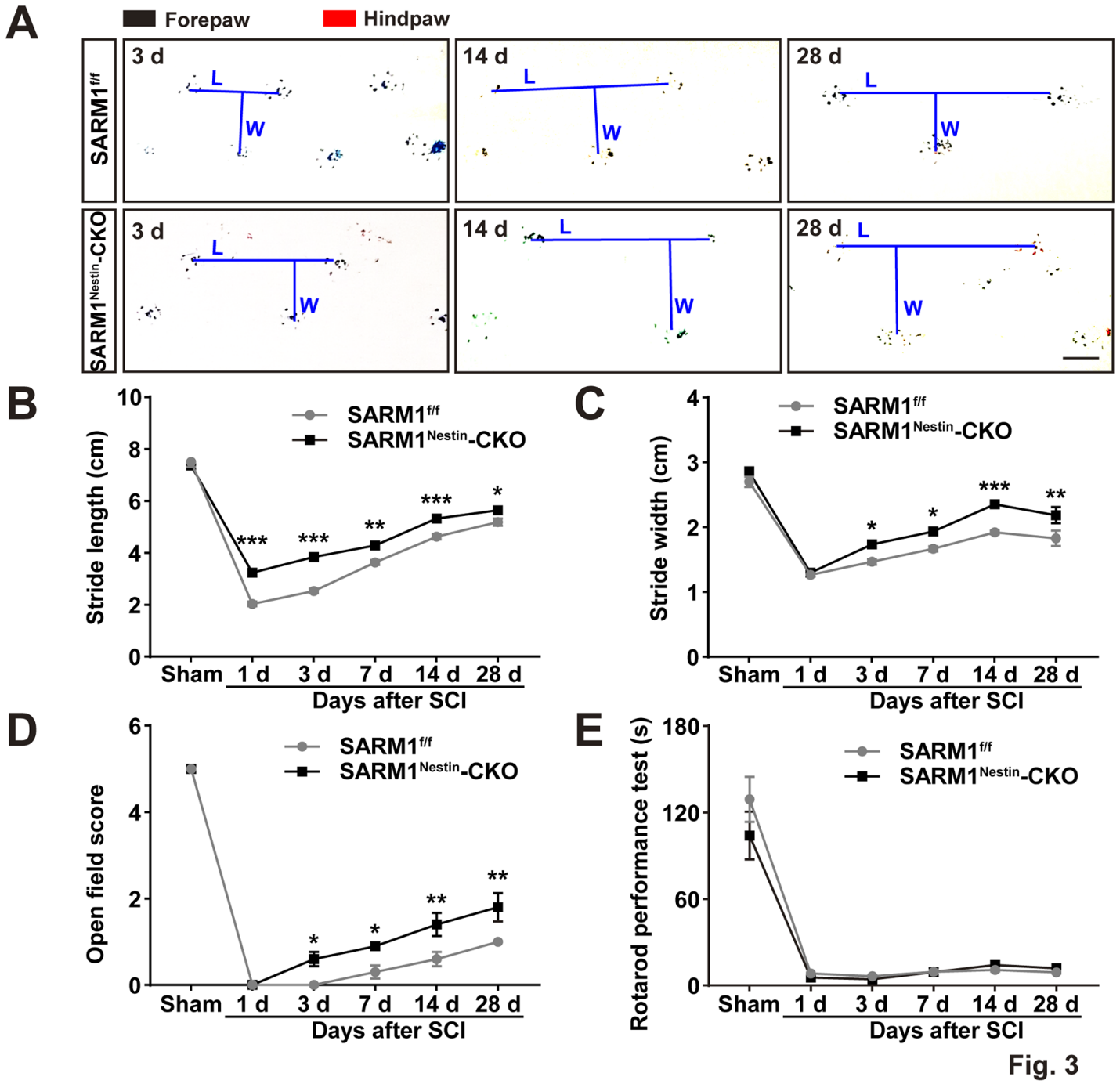

Figure 3

Conditional deletion of SARM1 in neurons promoted the recovery of behavior perfor-mance after SCI. (A) Representative footprint images of SARM1f/f and SARM1Nestin-CKO mice at 3 d, 14 d, 28 d after SCI. (B-C) Quantitative footprint analysis of stride length (B) and stride width (C) in footprint behavioral assay at different stages of SARM1f/f and SARM1Nestin-CKO mice after SCI (two-way ANOVA with Bonferroni's post-tests, n = 6 per group). (D-E) Quantitative analysis of gross voluntary movement in open-field walking (D, n = 10 per group) and time taken to fall in rotarod assays (E, n = 15 per group) of SARM1f/f and SARM1Nestin-CKO mice over a 28-d period after SCI (two-way ANOVA with Bonferroni's post-tests). Scale bars, 1 cm. Data were mean ± SEM. *P < 0.05, **P < 0.01, ***P < 0.001.

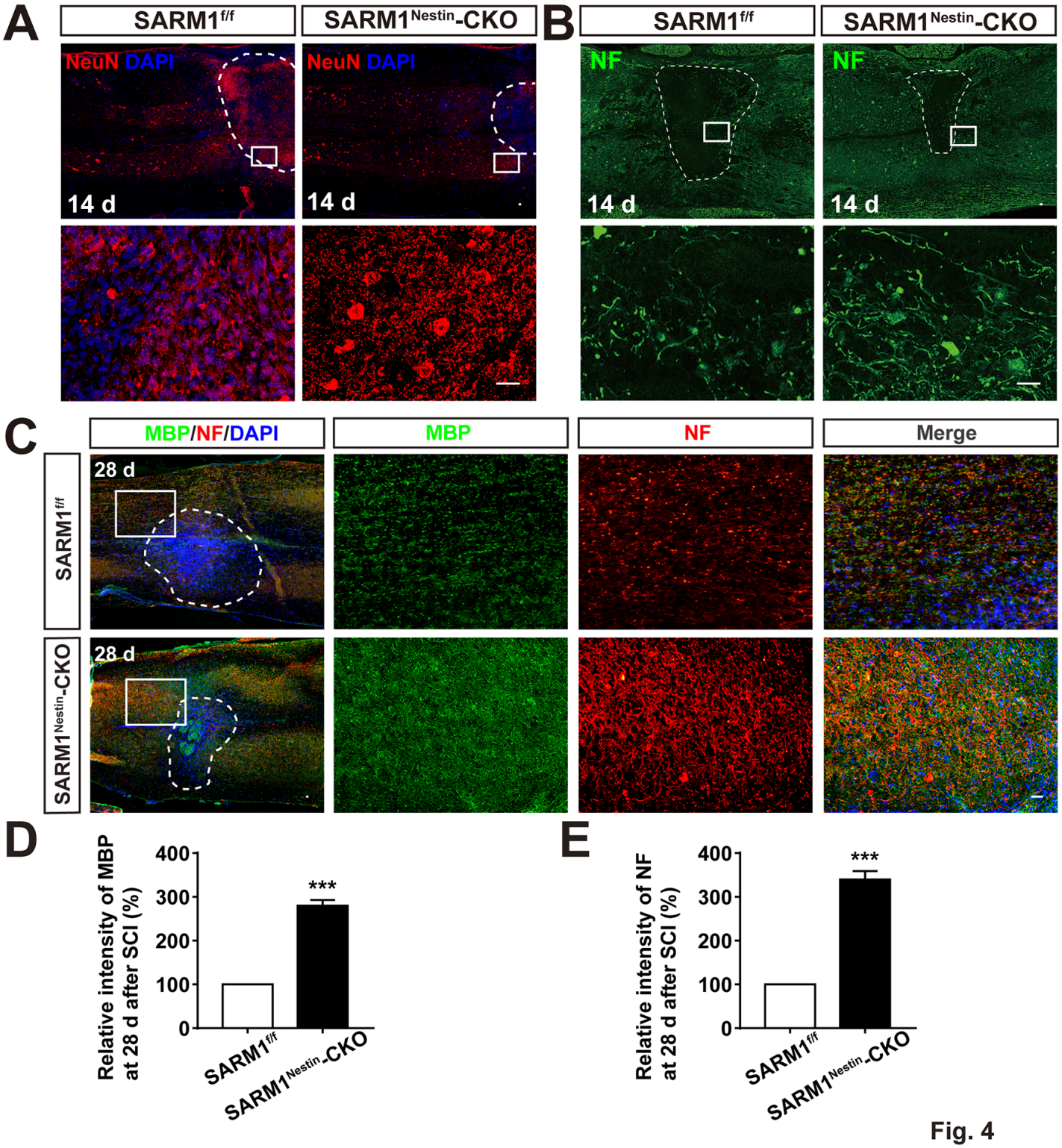

Figure 4

Conditional deletion of SARM1 in neurons promoted the neuronal regeneration at in-termediate phase after SCI. (A) Double immunostaining analysis of NeuN (red) and DAPI (blue) in the spinal cords of SARM1f/f and SARM1Nestin-CKO mice at 14 d after SCI. (B) Double immunostaining analysis of NF (green) in the spinal cords of SARM1f/f and SARM1Nestin-CKO mice at 14 d after SCI. (C) Double immunostaining analysis of MBP (green) and NF (red) in the spinal cords of SARM1f/f and

SARM1Nestin-CKO mice at 28 d after SCI. (D) Quantitative analysis of the in-tensity of MBP as shown in (C) (two-tailed unpaired Student's t-test, n = 6 per group, nor-malized to SARM1f/f mice group). (E) Quantitative analysis of the intensity of NF as shown in (C) (two-tailed unpaired Student's t-test, n = 6 per group, normalized to SARM1f/f mice group). Dashed lines indicated the outline of the injury sites. Images of selected regions (rectangles) in (A-C) were shown at higher magnification. Scale bars, 20 μm. Data were mean ± SEM. ***P < 0.001.

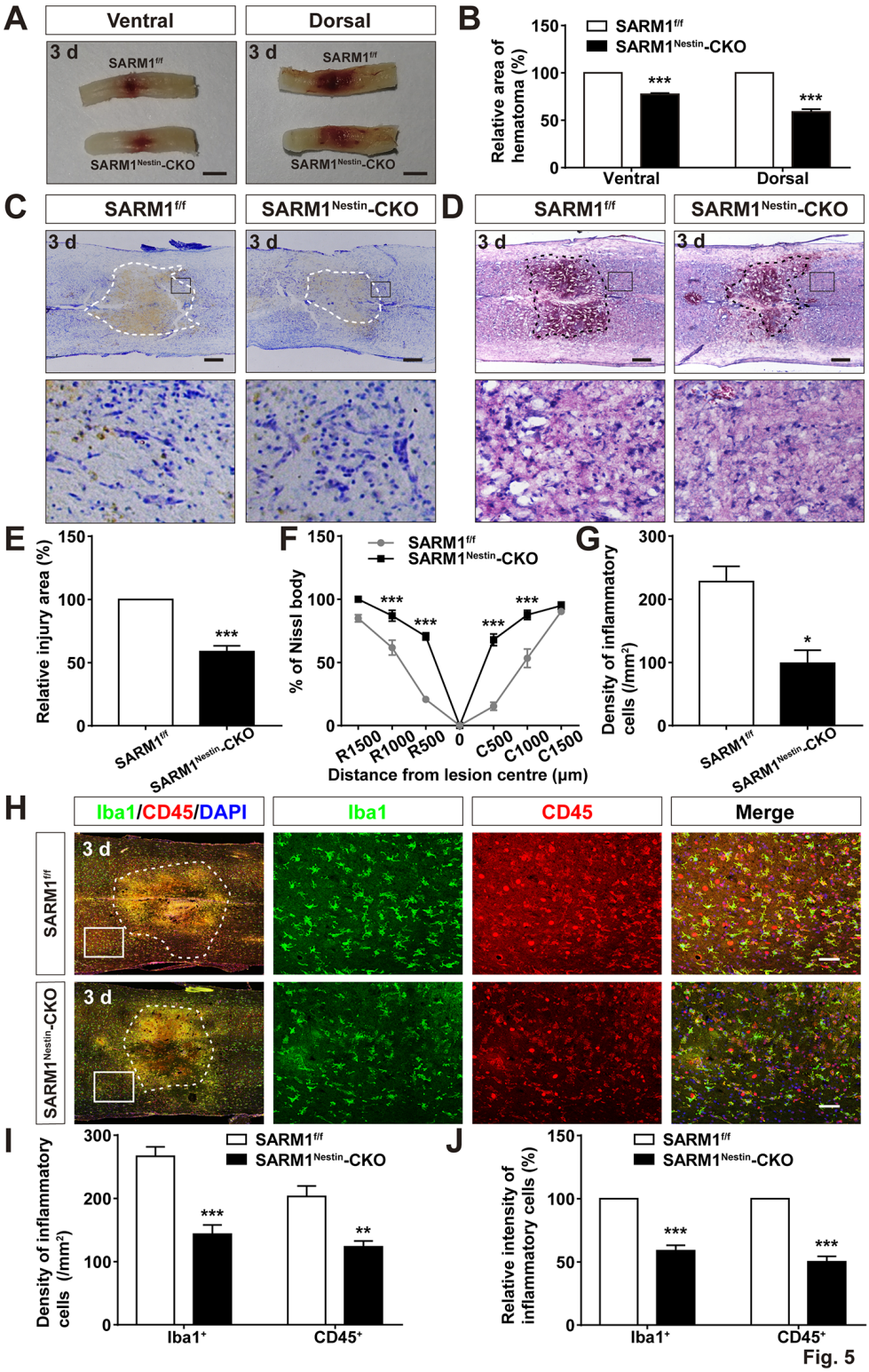

Figure 5

Conditional deletion of SARM1 in neurons reduced neuroinflammation at SCI early phase. (A) Representative images of the ventral and dorsal spinal cords with hematoma of SARM1f/f and SARM1Nestin-CKO mice at 3 d after SCI. (B) Quantitative analysis of hematoma area of the spinal cords as shown in (A) (two-tailed unpaired Student's t-test, n = 6 per group, nor-malized to SARM1f/f mice group). (C) Nissl staining images showing the injury area in the spinal cords of SARM1f/f and SARM1Nestin-CKO mice at 3 d after SCI. (D) HE staining images showing the inflammatory infiltration of the spinal cords of SARM1f/f and SARM1Nestin-CKO mice at 3 d after SCI. (E) Quantitative analysis of the injury area in the spinal cords as shown in (C) (two-tailed unpaired Student's t-test, n = 3 per group, normalized to SARM1f/f mice group). (F) Quantitative analysis of neurons by Nissl staining at various distances from the SCI lesion center as shown in (C) (two-way ANOVA with Bonferroni's post-tests, n = 3 per group, normalized to SARM1f/f mice group). (G) Quantitative analysis of the density of in-flammatory cells in the spinal cords as shown in (D) (two-tailed unpaired Student's t-test, n = 3 per group). (H) Double immunostaining analysis of Iba1 (green) and CD45 (red) in the spinal cords of SARM1f/f and SARM1Nestin-CKO mice at 3 d after SCI. (I) Quantitative analy-sis of the density of Iba1+ cells and CD45+ cells as shown in (H) (two-tailed unpaired Stu-dent's t-test, n = 6 per group). (J) Quantitative analysis of the intensity of Iba1+ cells and CD45+ cells as shown in (H) (two-tailed unpaired Student's t-test, n = 6 per group, normal-ized to SARM1f/f mice group). Dashed lines indicated the outline of the injury sites. Images of selected regions (rectangles) in (C, D, H) were shown at higher magnification. Scale bars, 3 mm (A), 20 μm (C, D, H). Data were mean ± SEM. *P < 0.05, **P < 0.01, ***P < 0.001.

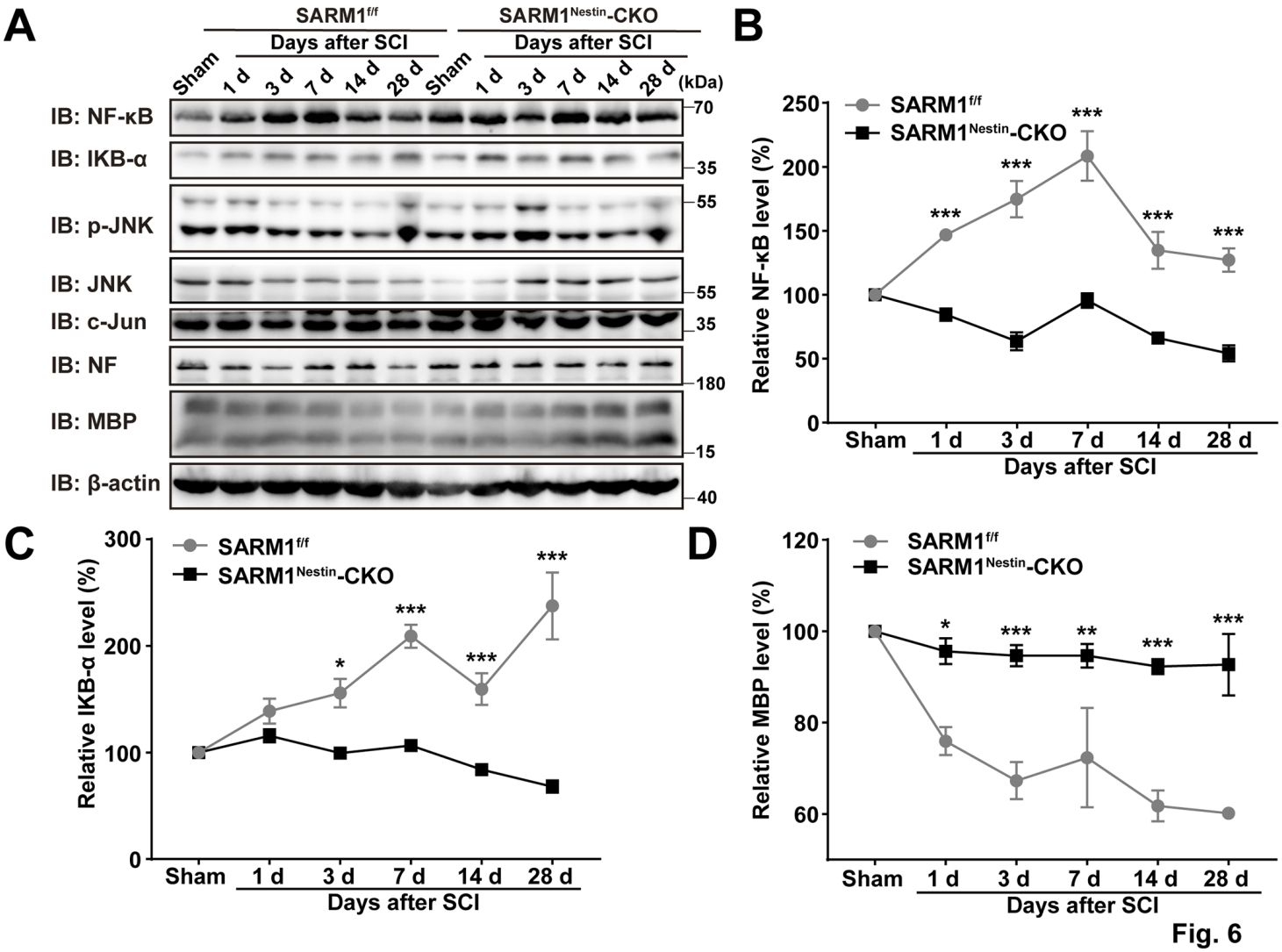

Fig. 6

Figure 6

Conditional deletion of SARM1 in neurons reduced the neuroinflammation through downregulation of NF-κB signaling after SCI. (A) Western blot analysis of the expression of NF-κB, IKB-α, NF, p-JNK, JNK, c-Jun and MBP in the spinal cords of SARM1f/f and SARM1Nestin-CKO mice at different stages after SCI. (B-D) Quantitative analysis of the relative NF-κB (B), IKB-α(C) and MBP (D) levels as shown in (A) (two-way ANOVA with Bonferroni's post-tests, n = 3 per group, normalized to sham group). Data were mean ± SEM. *P < 0.05, **P < 0.01, ***P < 0.001.

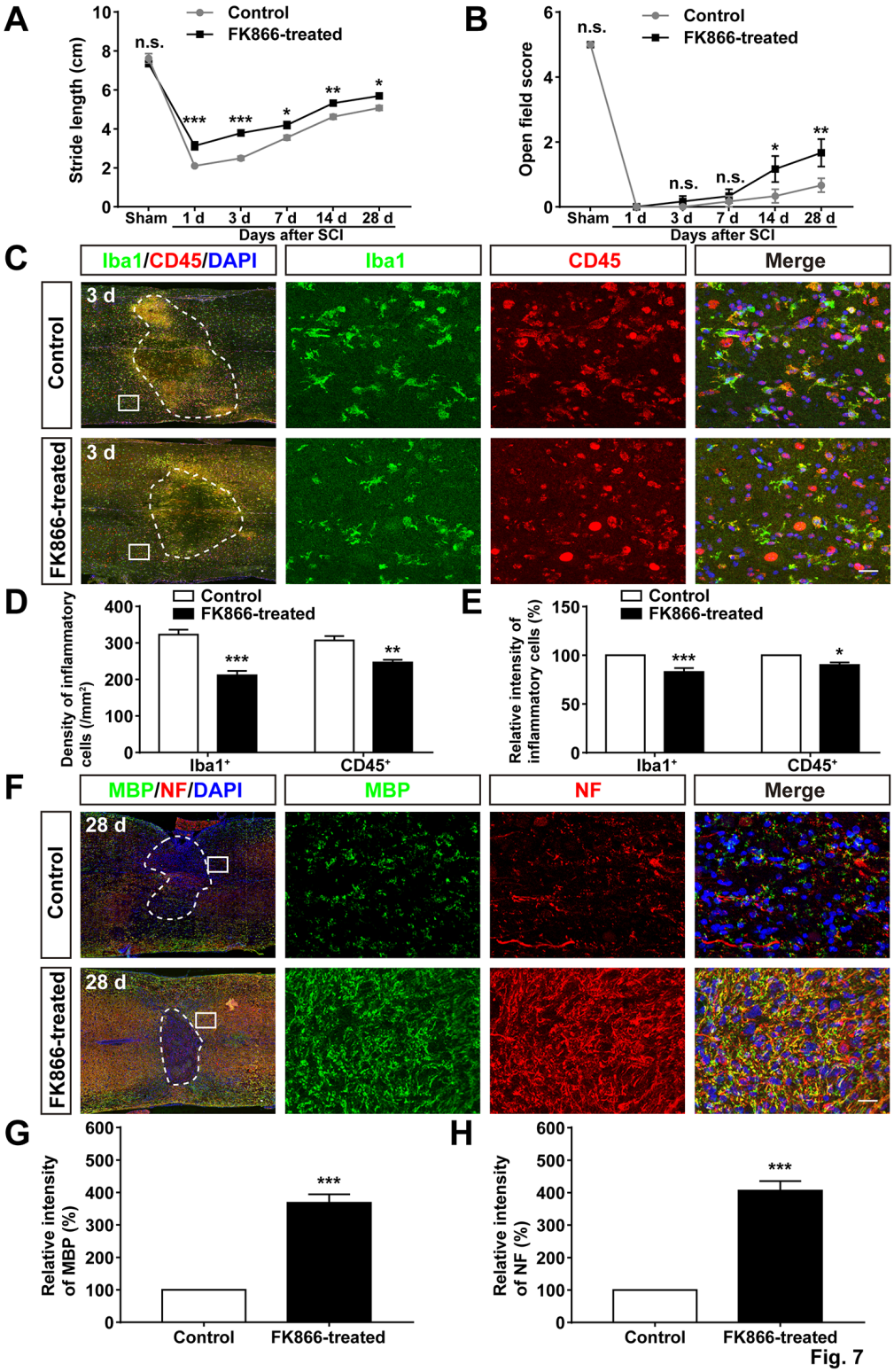

Figure 7

Inhibition of SARM1 by FK866 promoted neuronal regeneration after SCI. (A) Quantitative analysis of stride length in footprint assays at different stages of control (sa-line-treated) and FK866-treated mice after SCI (two-way ANOVA with Bonferroni's post-tests, n = 4 per group). (B) Quantitative analysis of gross voluntary movement in the open field test of control and FK866-treated mice in open-field walking assays over a 28-d period after SCI (two-way ANOVA with Bonferroni's post-tests, n = 6 per group). (C) Dou-ble

immunostaining analysis of Iba1 (green) and CD45 (red) in spinal cords of control and FK866-treated mice at 28 d after SCI. (D) Quantitative analysis of the density of Iba1+ cells and CD45+ cells as shown in (C) (two-tailed unpaired Student's t-test, n = 6 per group). (E) Quantitative analysis of the intensity of Iba1+ cells and CD45+ cells as shown in (C) (two-tailed unpaired Student's t-test, n = 6 per group, normalized to control mice group). (F) Double immunostaining analysis of MBP (green) and NF (red) in control and FK866-treated spinal cords at 28 d after SCI. (G) Quantitative analysis of the intensity of MBP as shown in (F) (two-tailed unpaired Student's t-test, n = 3 per group, normalized to control mice group). (H) Quantitative analysis of the intensity of NF as shown in (F) (two-tailed unpaired Stu-dent's t-test, n = 3 per group, normalized to control mice group). Dashed lines indicated the outline of the injury sites. Images of selected regions (rectangles) in (C) and (F) were shown at higher magnification. Scale bars, 20 μm (C, F). Data were mean ± SEM. n.s., not signifi-cant (P > 0.05), *P < 0.05, **P < 0.01, ***P < 0.001.

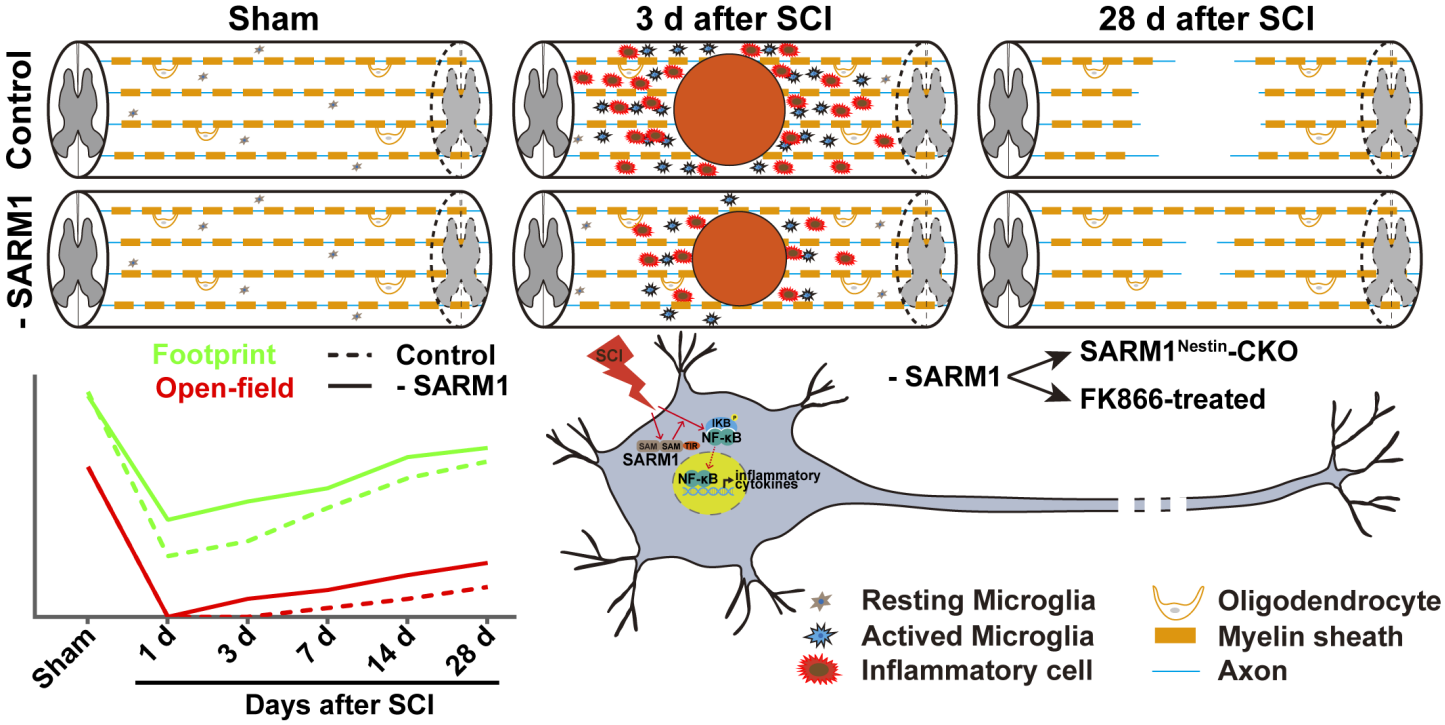

Fig. 8

Figure 8

A working model of SARM1's function after SCI. Conditional deletion of SARM1 in neurons or FK866 treatment inhibited the generation of neuroinflammation cells, promoted the axonal regeneration, and improved the behavioral recovery of motor function through downregulation of NF-κB signaling after SCI.

Supplementary Files

This is a list of supplementary files associated with this preprint. Click to download.

- SupplementaryFig.1.tif
- SupplementaryFig.1.tif

- SupplementaryFig.4.tif
- SupplementaryFig.4.tif
- SupplementaryFig.2.tif
- SupplementaryFig.2.tif
- SupplementaryFig.5.tif
- SupplementaryFig.5.tif
- SupplementaryFig.3.tif
- SupplementaryFig.3.tif